On the Similitude Between Lifted and Burner-Stabilized Triple Flames: A Numerical and Experimental Investigation

ISHWAR K. PURI,* SURESH K. AGGARWAL, STEFANO RATTI, and RICCARDO AZZONI

Department of Mechnical Engineering (M/C 251), University of Illinois at Chicago, 842 W. Taylor St., RM 2039, Chicago, IL 60607-7022, USA

We have investigated lifted triple flames and addressed issues related to flame stabilization. The stabilization of nonpremixed flames has been argued to result due to the existence of a premixing zone of sufficient reactivity, which causes propagating premixed reaction zones to anchor a nonpremixed zone. We first validate our simulations with detailed measurements in more tractable methane–air burner-stabilized flames. Thereafter, we simulate lifted flames without significantly modifying the boundary conditions used for investigating the burner-stabilized flames. The similarities and differences between the structures of lifted and burner-stabilized flames are elucidated, and the role of the laminar flame speed in the stabilization of lifted triple flames is characterized. The reaction zone topography in the flame is as follows. The flame consists of an outer lean premixed reaction zone, an inner rich premixed reaction zone, and a nonpremixed reaction zone where partially oxidized fuel and oxidizer (from the rich and lean premixed reaction zones, respectively) mix in stoichiometric proportion and thereafter burn. The region with the highest temperatures lies between the inner premixed and the central nonpremixed reaction zone. The heat released in the reaction zones is transported both upstream (by diffusion) and downstream to other portions of the flame. Measured and simulated species concentration profiles of reactant (O_2, CH_4) consumption, intermediate (CO, H_2) formation followed by intermediate consumption and product (CO_2, H_2O) formation are presented. A lifted flame is simulated by conceptualizing a splitter wall of infinitesimal thickness. The flame liftoff increases the height of the inner premixed reaction zone due to the modification of the upstream flow field. However, both the lifted and burner-stabilized flames exhibit remarkable similarity with respect to the shapes and separation distances regarding the three reaction zones. The heat-release distribution and the scalar profiles are also virtually identical for the lifted and burner-stabilized flames in mixture fraction space and attest to the similitude between the burner-stabilized and lifted flames. In the lifted flame, the velocity field diverges upstream of the flame, causing the velocity to reach a minimum value at the triple point. The streamwise velocity at the triple point is ≈ 0.45 m s^{-1} (in accord with the propagation speed for stoichiometric methane–air flame), whereas the velocity upstream of the triple point equals 0.7 m s^{-1}, which is in excess of the unstretched flame propagation speed. This is in agreement with measurements reported by other investigators. In future work we will address the behavior of this velocity as the equivalence ratio, the inlet velocity profile, and inlet mixture fraction are changed.   © 2001 by The Combustion Institute

INTRODUCTION

Our previous investigations of laminar triple flames [1, 2] have focussed on burner-stabilized flames due to two-considerations. First, it is difficult to stabilize a two-dimensional lifted triple flame on a laboratory slot burner due to edge effects that cause lifted flames to have a bow shape in the cross-stream direction. Consequently, the flames are lifted higher along the burner edges than the middle. This has prevented a comparison over a wide range of parametric conditions of measurements with simulations, which are based on a two-dimensional computational algorithm. Second, under

a variety of conditions, a burner-stabilized triple flame is relatively more stable and, therefore, less sensitive to ambient perturbations in the laboratory than a corresponding lifted flame. Hence, the choice of a burner-stabilized flame made it easier for us to conduct a detailed parametric study that clarified the effects of velocity and local equivalence ratio on the flame structure based on both simulations and experiments [1, 2]. Although our previous investigations have enhanced the understanding of the chemical and transport-induced interactions between the various reaction zones that occur in triple flames, they did not directly address issues related to flame liftoff and stabilization.

Phillips first investigated the propagation of triple flames in a methane mixing layer that

---

*Corresponding author. E-mail: ikpuri@uic.edu

mimicked the roof of coal mine roadways [3]. It is now believed that these flames can play an important role in the stabilization of laminar nonpremixed flames [4]. While premixed flames propagate (and stabilize) due to heat transport from the burned to the unburned mixture, nonpremixed flames do not possess such a simple stabilization mechanism in the vicinity of a cold surface. A common view of nonpremixed flame stabilization proposed by Takahashi and Katta [5] focuses on the upstream mass transport of radicals from a reaction kernel that represents a region of high reactivity. This radical flux is believed to increase the chemical reaction rates for important reaction steps near a stabilization point that is located in a small premixing zone. Wichman and Ramadan [6] state that, on the contrary, upstream radical transport is not a necessary condition, and that flame stabilization can result just due to the existence of a premixing zone of sufficient reactivity. Chung and Lee [7] offer two examples of nonpremixed flame stabilization. One pertains to the near region of a splitter plate in which the wake, which provides low strain rates for mixing and heat conduction from the flame to the plate, becomes important in the manner of a premixed flame. Their other illustration pertains to flames that are lifted downstream in the form of a triple flame. Here, the propagating premixed reaction zones anchor a nonpremixed zone [7].

Although many arguments have been proposed to explain nonpremixed flame stabilization, most agree that (partial) premixing and the synergistic interactions between various reaction zones play a key role. Echekki and Chen [8] conducted direct numerical simulations, and concluded that both the curvature and diffusion effects augment radical production that, consequently, enhances the flame propagation speed. Aggarwal and Puri [9] have determined the existence of triple flames in relatively complex configurations. The structure of these flames has been characterized in detail by Azzoni et al. [1, 2] and Plessing et al. [10]. Buckmaster and Matalon [11] have also investigated transport effects on these flames. Domingo and Vervisch [12] have suggested that the front of a triple flame can propagate because of the interaction of multiple rich and lean layers, in accord with the conclusions of Aggarwal and Puri [9]. Par-

tial premixing and triple flames are also important in the case of initially nonpremixed turbulent flames that are highly stretched when, after a local extinction, the turbulence intensity decreases and allows reignition, again in a lifted-like configuration [13]. Evidence of this phenomenon is provided by Ratner et al. [14] through an experimental investigation of highly wrinkled turbulent nonpremixed flames.

Objective

We have previously reported on the structure and dynamics of stable burner-stabilized triple flames [1, 2]. Our objective herein is to examine the similitude between stable lifted triple flames and their burner-stabilized counterparts. We first validate our simulations with measurements in the more tractable burner-stabilized flames. Thereafter, we simulate lifted flames without significantly modifying the boundary conditions used for investigating the burner-stabilized flames. The similarities and differences between the structures of lifted and burner-stabilized flames are elucidated, and the effect of the laminar flame speed on the stabilization of lifted triple flames is characterized. This paper also provides a detailed comparison between measurements and predictions for partially premixed flames which, in addition to the previous comparison of the reaction zone topology and velocity [1, 2], includes comparisons for temperature, and major species mol fractions. We also provide new computational results on lifted partially premixed flames, which highlight many fundamental features of these flames.

PROCEDURE

Atmospheric methane–air flames are established using a Wolfhard-Parker slot burner that contains ceramic inserts. The rectangular burner geometry provides symmetrical two-dimensional flames. Details of the burner can be found elsewhere [1, 15].

Temperature Measurements

Holographic interferometry can be used to obtain the temperature measurements in flames

[16–18]. We have used this technique to measure the temperature of two-dimensional slot burner flames. Our methodology is reported elsewhere in detail [19,20], so that only a brief description follows. A double-exposure laser image holographic process is used to measure the refractive index distribution. A typical off-axis holography system is used. The beam from a 17 mW He-Ne laser is divided by a beam splitter into an object and a reference beam. The object beam passes through the flame in the cross-stream direction that contains a two-dimensional refractive index distribution. The temperature is related to the refractive index through the relation $T = (n_0 - 1)T_0/(n_0 - (N\lambda)/L - 1)$, where N denotes the fringe number (inferred from the hologram image), n_0 the reference refractive index at the temperature T_0, λ the wavelength, and L the beam path integration length (in this case the burner dimension in the cross-stream direction).

Species Measurements

Gas chromatography is employed to determine the major species' concentrations, namely, H_2, N_2, O_2, CO, CO_2, and CH_4, in the flame. The species are sampled at various locations in the flame using a quartz microprobe. The sampling and analysis methods are described in detail elsewhere [21,22]. Water is not directly sampled, but its concentration can be inferred based on the assumption that the mass transport of C- and H-containing species are equal, i.e., the elemental mass fraction are related to the species mass fractions in the form $Z_i/W_i = \Sigma_{j=1,N} a_{ij} Y_i/W_i$. The implication of this assumption is that $Z_C/W_C = Z_H/4W_H$, where Z_i and W_I, respectively, represent the mass fraction and the molecular weight of element i. Because the concentrations of all major C- and H-containing species, except H_2O, are known, this relation is applied to determine the mass fraction of water.

Numerical Model

The computational model is based on the algorithm developed by Katta et al. [23]. An implicit algorithm is employed to solve the unsteady gas-phase equations. The simulation method is described in detail elsewhere [12, 15, 24, 25]. The numerical model solves the time-dependent governing equations for a two-dimensional reacting flow. Using Cartesian coordinates (x, y), these equations representing the mass, momentum, species, and energy conservation equations, can be written in the form

$$\frac{\partial(\rho\phi)}{\partial t} + \frac{\partial(\rho u\phi)}{\partial x} + \frac{\partial(\rho v\phi)}{\partial y} = \frac{\partial}{\partial x}\left(\Gamma^\phi \frac{\partial\phi}{\partial x}\right)$$

$$+ \frac{\partial}{\partial y}\left(\Gamma^\phi \frac{\partial\phi}{\partial y}\right) + S^\phi, \tag{1}$$

where ρ denotes density, and u and v the transverse (x) and streamwise (y) velocity components, respectively. The transport coefficient Γ^ϕ and the source terms S^ϕ appearing in the governing equations are provided in Table 1 of Ref. [24]. The set of equations is completed by introducing the mass conservation equation and the state equation $p = \rho R_u T P_i Y_i/M_i$ (where R_u denotes the universal gas constant, T the temperature, and M_i the molecular weight of the i-the species). The thermodynamic and transport properties appearing in the above equations are considered to be temperature and species dependent. The methodology to calculate these properties is based on Chapman-Enskog collision theory, the Lennard-Jones potentials, and the Wilke semiempirical formulae. The enthalpy h and specific heats are based on fits from [26]. The methane–air chemistry is modeled using a detailed model that considers 24 species and 81 elementary reactions [27].

The computational domain is bounded by the symmetry plane and an outflow boundary in the transverse direction and by the inflow and another outflow boundary in the streamwise direction. Symmetric conditions are applied at the left boundary, whereas those at right boundary correspond to a free surface. The outflow boundaries in both directions are located sufficiently far from the respective inflow and symmetric boundaries so that the propagation of boundary-induced disturbances is minimized. The boundary conditions are chosen to match the experiments. The governing equations are integrated by using a "finite control volume" approach with a staggered, nonuniform 131 × 88 grid system.
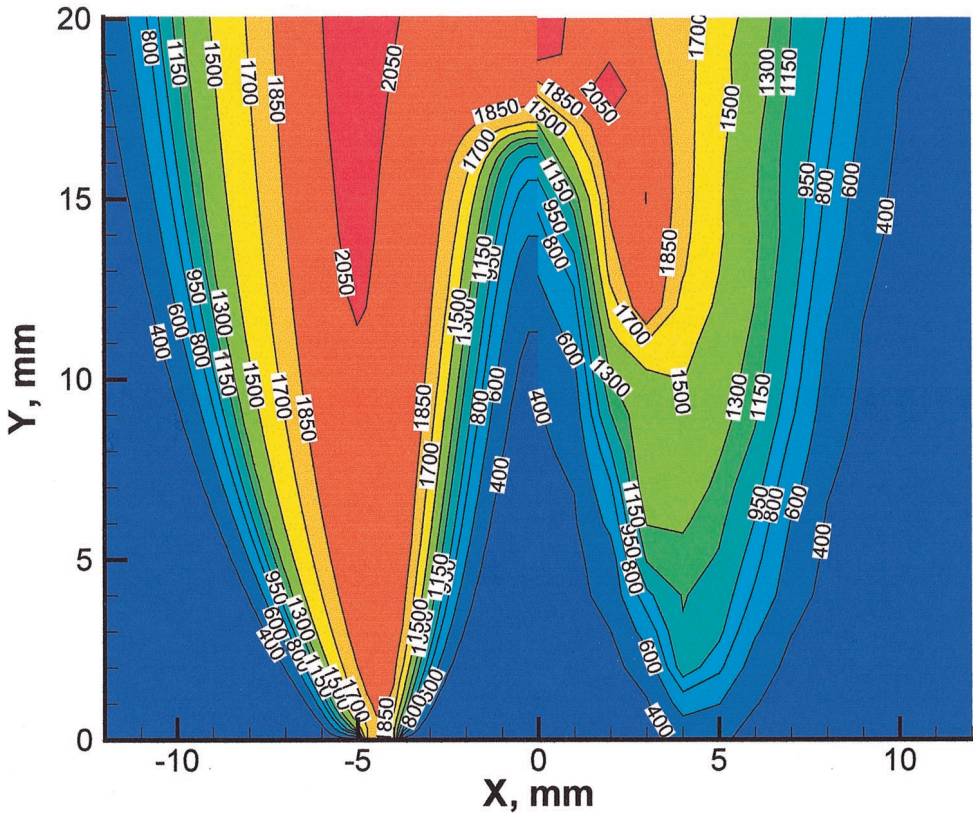
Fig. 1. Comparison between predicted (left) and measured (right) temperature distribution for a burner-stabilized triple flame flame. The triple flame is established at an overall equivalence ratio $\phi_{overall} = 0.6$, inner equivalence ratio inner equivalence ratio $\phi_{in} = 1.8$, outer equivalence ratio $\phi_{out} = 0.35$, and bulk-averaged velocities equal to 0.3 m s^{-1} through both slots. A qualitative comparison of this data is contained elsewhere [1].

RESULTS AND DISCUSSION

Global Flame Structure

Partial validation of the computational code in terms of the reaction zone topography and the flow velocities has already been presented earlier [1]. A plug flow velocity was assumed at the inlet boundary. We have previously reported good agreement with the measured C_2^* chemiluminescence emission intensity, which is a good indicator of the reaction zone topology and the computed volumetric heat release rate for a representative burner-stabilized flame [15, 28, 29]. That analysis followed the methodology in Shu et al. [15], who performed a detailed investigation of the relationship between the flame heat release rate and the C_2^* chemiluminescence intensity emission.

The reaction zone topography in the steady laminar flame is as follows. The flame is symmetric with respect to the vertical direction. It consists of an outer lean premixed reaction zone, an inner rich premixed reaction zone, and a nonpremixed reaction zone where partially oxidized fuel and oxidizer (from the rich and lean premixed reaction zones, respectively) mix in stoichiometric proportion and thereafter burn. The predicted flame shape is in excellent agreement with the spatial profile of the measured chemiluminescence intensity. The height of the inner reaction zone is well predicted, and the measured and predicted shapes and widths of the two outer (nonpremixed and lean premixed) reaction zones are in good agreement. Readers are referred to Ref. [1] for a visual description of the three reaction zones.

Figure 1 presents a comparison between the holography temperature measurements and the numerical predictions for the flame in a 12 ×

20-mm area immediately above the burner, which contains all three reaction zones, and the triple point where they merge. We have previously presented a qualitative comparison of the data contained in Fig. 1 [1]. The measurements and predictions are in excellent agreement, although despite the absence of a thermal radiation model in the simulations the measured maximum temperature is $\approx$100 K higher (2195 K vs. 2089 K in the predictions). This discrepancy in the measured temperature is attributed to uncertainties in the measurements and the model (e.g., related to the chemical mechanism, and the thermophysical and transport properties). We have previously shown that the average error involved in the inference of the temperature of partially premixed flames from holographic interferometry measurements is less than 5%, and that the maximum error anywhere in the domain is less than 10% [20]. In general, the maximum error lies not in the high-temperature region, but on the rich side of the flame where the local temperatures are far smaller. The measured temperatures downstream of the stabilization increase more gradually in comparison with the predictions, and are up to a factor of 2 lower in the first few millimeters following the burner inlet. We attribute these discrepancies to the small heat transfer to the laboratory burner, differences in the inlet velocity profiles in the experiment and computations (cf. [1]), and to uncertainties in the chemistry model.

The high-temperature region appears to be slightly narrower in the laboratory flame due to burner edge effects. This will be corroborated by the species concentration measurements. The hotter regions do not necessarily correspond to regions of high chemical activity, because the heat released in the reaction zones is transported both upstream (by diffusion) and downstream to other portions of the flame. In both the measurements and predictions, the region with the highest temperatures lies between the inner premixed and the central nonpremixed reaction zone.

There is a finite temperature gradient towards the burner edge, implying that some heat is being transferred from the flame. The simulated results show that the high-temperature region is established immediately after the burner exit. However, lower temperatures (in the range of 400–450 K) are measured in the vicinity of the burner exit. This discrepancy arises because the model does not account for the burner heat loss. We have earlier induced this heat loss from the measurements and found it to be less than 0.5% of the maximum possible heat release (1.15 kW) from the flame [1].

Regardless of this difference in the measured and predicted temperatures in the upstream region, there is good qualitative and quantitative agreement at other downstream locations. Both the simulations and the predictions indicate a thin reaction zone. Within the bounds of computational and experimental errors, there is good agreement between the measured and predicted temperatures along the center line. This indicates that the small amount of heat transfer near the stabilization point does not have a significant global impact on the triple flame.

Measured and predicted streamwise species concentration profiles for the burner-stabilized flame are presented in Figs. 2–7 for five transverse displacements (namely, x = 0, 2, 4, 6, and 10 mm), respectively, for O_2, CO, CO_2, CH_4, H_2, and H_2O. The uncertainties involved in the measurements lie between 5–10%. The species have scalar profiles that represent reactant (CH_4, O_2) consumption, intermediate (H_2, CO) formation followed by intermediate consumption, and product (H_2O, CO_2) formation. The measurements further validate the numerical model and provide insight into the flame structure.

Figure 2 shows streamwise profiles of oxygen concentration for the flame. There is a reasonable agreement between the measurements and the predictions at the different locations. The sharp change in the oxygen concentration marks the location of the inner rich premixed reaction zone along x = 0 mm. This reaction zone moves to lower displacements at x = 2 and 4 mm in accord with the curved shape of the inner flame. The profile along x = 6 mm spatially crosses the outer lean premixed reaction zone and is almost parallel to the nonpremixed reaction zone. The oxygen content is, consequently, small. At x = 10 mm, the vertical displacements are located in regions of low chemical activity outside the overall flame, and the oxygen concentration
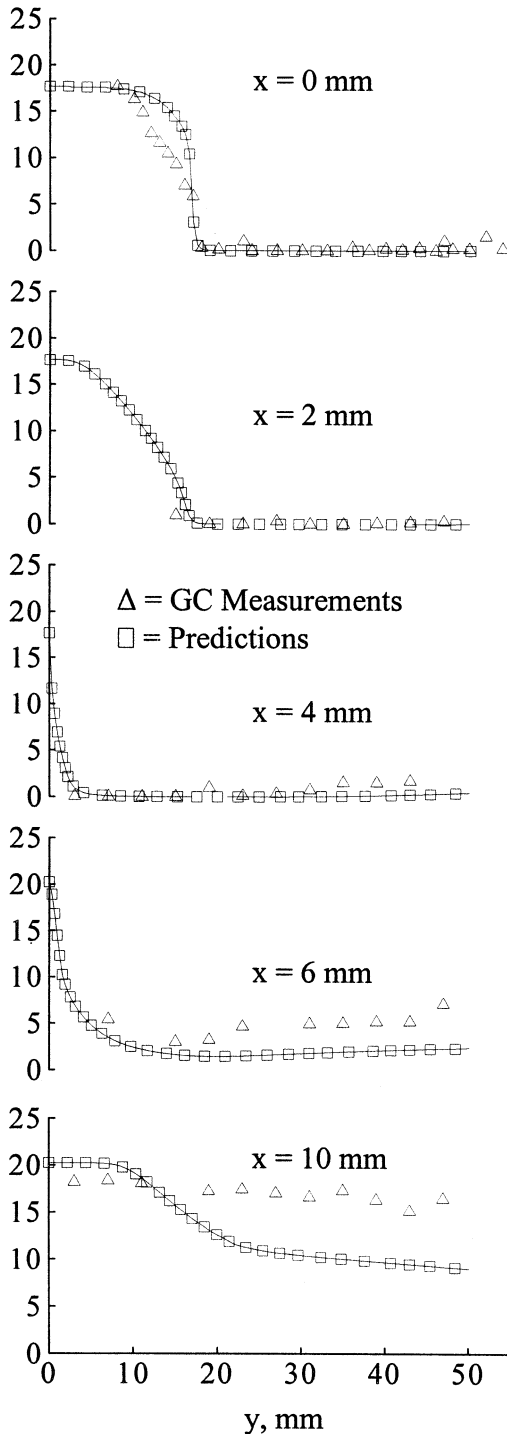
Fig. 2. Streamwise profiles of the oxygen mass percentage at different transverse displacements for the flame discussed in context of Fig. 1.

reaches ambient levels. The measurements suggest that the laboratory flame is thinner in the transverse direction, which is most likely due to edge effects.

The CO profiles (presented in Fig. 3) are also in good agreement with the numerical predictions. Higher concentrations of CO occur in the inner premixed reaction zone, downstream of which CO is depleted as it is transported to the nonpremixed reaction zone in which it is consumed and forms CO_2. The carbon monoxide peaks in the vicinity of the inner rich premixed reaction zone are clearly distinguishable at various vertical displacements at x = 0, 2, and 4 mm. No CO is present along the two outermost transverse displacements, even though the lean premixed reaction zone is crossed over at some streamwise (vertical) positions. This clearly shows that CO is an intermediate species that is formed where rich combustion occurs, and is consumed in a nonpremixed reaction zone. The corresponding CO_2 concentration (presented in Fig. 4) increases across the inner reaction zone and thereafter due to carbon monoxide conversion. This trend is clear at x = 0, 2 and 4 mm and is in accord with the numerical predictions, even though some quantitative discrepancies are present. At higher locations the CO_2 concentration is underpredicted.

The discrepancies arise due to two reasons—one due to the dilution of the gases above the burner through a small ambient cross wind and edge effects; the other reason is the small differences in the measured and predicted locations of the rich premixed and nonpremixed reaction zone, which, respectively, correspond to locations with the largest CO and CO_2 concentrations.

Figure 5 presents the methane concentrations in the flame. The measurements are generally in agreement with the predictions. However, the laboratory flame again appears to be thinner than the predictions imply. A discrepancy is apparent at vertical displacements along x = 10 mm, where the measurements show that methane is not completely consumed, but reaches a constant value that is very close to that introduced through the outer slot. In contrast, the predictions show that methane is completely burned within the first two centimeters following the burner exit. The far-field discrepancy is
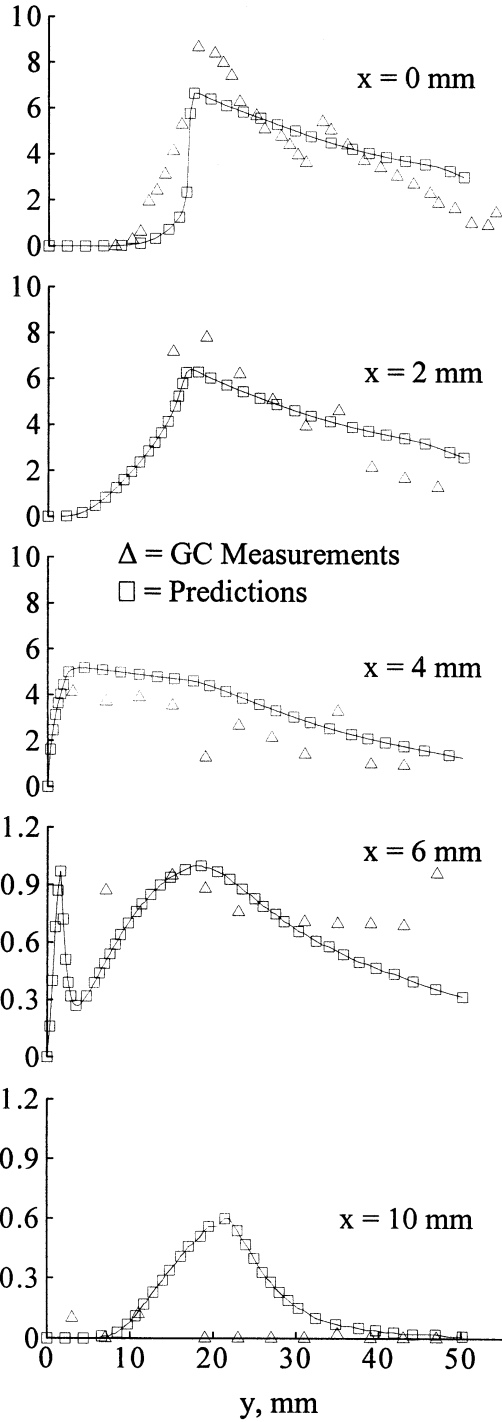
Fig. 3. Streamwise profiles of the carbon monoxide mass percentage at different transverse displacements for the flame discussed in context of Fig. 1.
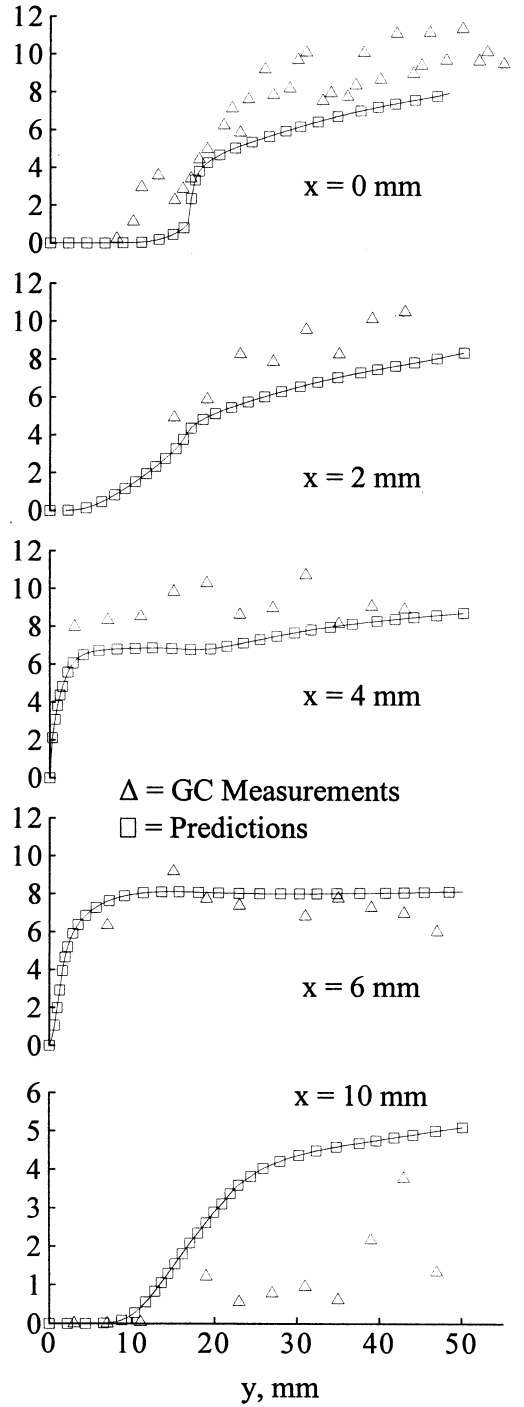
Fig. 4. Streamwise profiles of the carbon dioxide mass percentage at different transverse displacements for the flame discussed in context of Fig. 1.
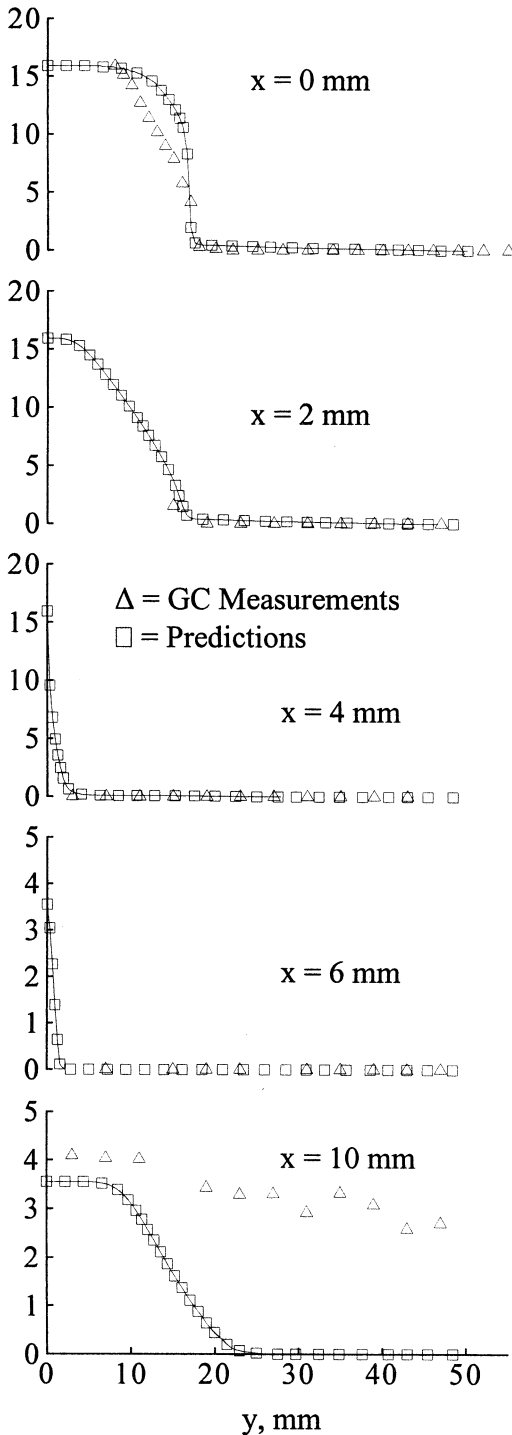
Fig. 5. Streamwise profiles of the methane mass percentage at different transverse displacements for the flame discussed in context of Fig. 1.

attributed to the effects of ambient disturbances in the laboratory ventilation. Although the flame is shielded from the ambient by a containing metal wire mesh, it is possible for disturbances to influence the flame, although in a greatly attenuated form.

The concentration profiles of molecular hydrogen are presented in Fig. 6. The measurement error associated with hydrogen is significant, because it has a low molecular weight, and its low mass fraction in the samples induces small changes in the mixture thermal conductivity. As a result, the hydrogen peaks in the chromatographs are very small, and measurement noise becomes significant and, consequently, the H_2 measurements are unfortunately less reliable. Therefore, the qualitative agreement between the measurements and predictions is significant. The H_2 concentration reaches a maximum in the inner premixed reaction zone and then decreases. Molecular hydrogen is not present at higher locations or outside of the overall flame at x = 6 and 10 mm. This trend is similar to that exhibited by carbon monoxide, because both species are intermediate species and are ultimately consumed to form carbon dioxide and H_2O.

Finally, Fig. 7 presents the water concentration profiles that were deduced using the assumption that the mass transport of the C- and H-containing species are equal. Water is underpredicted close to the center line and overpredicted at transversely outward locations. This is consistent with the discrepancies in the other measurements that the laboratory flame is slightly more compact than that which is predicted (and in accordance with the temperature measurements discussed earlier).

Although we note the overall agreement between the measured and predicted mol fractions, we note the existence of local differences. For instance, the predicted O_2 profiles are in some areas much lower than the measurements, and cross stream disturbances and edge effects raise this discrepancy. The chemistry model also contributes to these differences, because it indicates that methane consumption at the edges is lower than that predicted.

The data presented in Figs. 2–7 allow us to decipher the flame structure. Both the measurements and predictions show that molecular hy-
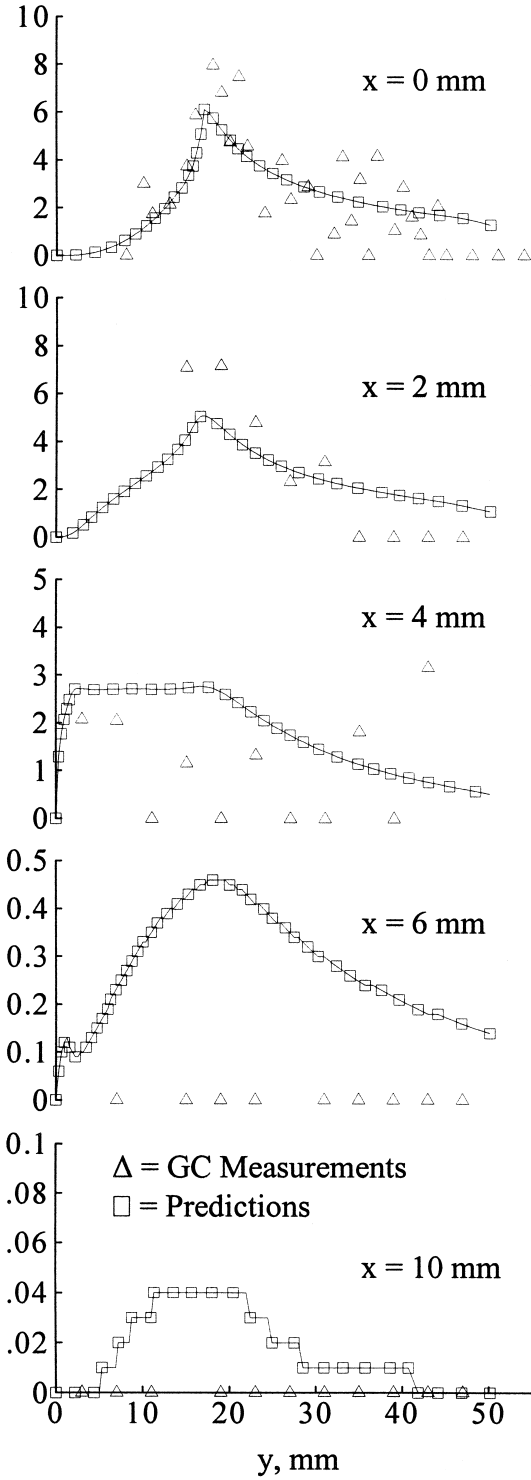
Fig. 6. Streamwise profiles of the molecular hydrogen mass percentage at different transverse displacements for the flame discussed in context of Fig. 2.
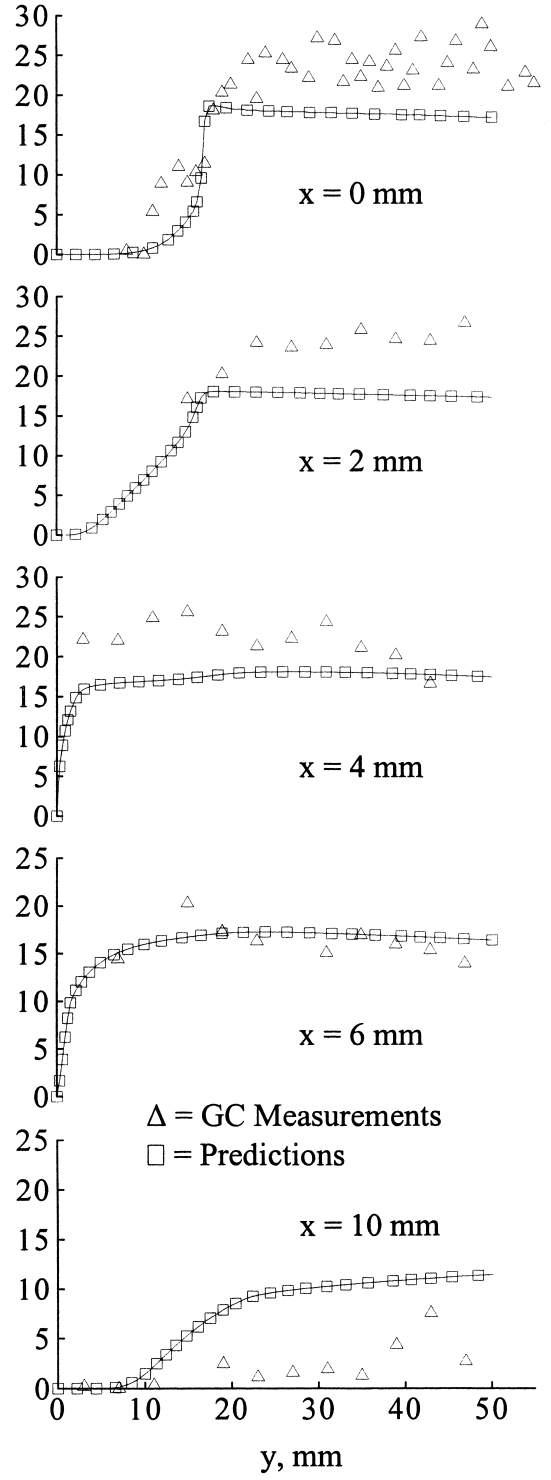
Fig. 7. Streamwise profiles of the water mass percentage at different transverse displacements for the flame discussed in context of Fig. 2.

drogen and carbon monoxide are mainly pro-
duced in the inner reaction zone, and both
species reach a maximum concentration in the
vicinity of the tip of that zone. They are then
transported toward the nonpremixed reaction
zone in which CO is oxidized into CO_2 and H_2
into H_2O. Excess O_2 leaks through the outer
lean premixed reaction zone, and is transported
toward the nonpremixed region. The nonpre-
mixed reaction zone is characterized by product
formation reactions, as opposed to the initiation
reactions that take place in the inner premixed
reaction zone. The nonpremixed reaction zone
also corresponds to high temperatures, which
cause a corresponding superequilibrium of rad-
ical species. The radicals produced in this zone
are transported to the other flame regions
where they initiate chemical reactions involving
the reactants.

Lifted Flame

Because we have simulated the burner-stabi-
lized flame with some confidence, we now focus
attention on the lifted flame. Figure 8 compares
the heat release rate profiles of two triple flames
simulated under identical stoichiometric and
inflow velocity conditions. The simulation con-
ditions are $\phi_{in} = 1.8$, $\phi_{out} = 0.35$, $v_{in} = v_{out} =$
0.7 m s^{-1} for both cases. The lifted flame is
obtained by creating a splitter wall of infinites-
imal thickness, whereas the burner-stabilized
flame has a corresponding 1.1 mm-thick splitter
plate. Although we realize that this thickness is
unrealistic from an experimental perspective, as
we will see later, the simulation provides inter-
esting insights into the lifted flame structure and
dynamics.

The lifted flame is located at a height of ≈ 4.5
mm from the burner. However, the height dif-
ference in the two rich premixed zones is ≈ 8.5
mm, which is attributed to the flame lift off that
modifies the upstream flow field and to the
increased slot width. Apart from this obvious
difference, the two flames exhibit a remarkable
similarity with respect to the overall topogra-
phy, i.e., the shapes and separation distances
regarding the three reaction zones. The triple
point for the burner-stabilized flame is located
in the wake of the splitter wall in close proximity
to the burner.

An important characteristic of the triple point
is the flame curvature at that location. This
curvature depends upon the inflow velocity and
equivalence ratio gradient. The triple point
influences the location and speed at which the
flame stabilizes through the divergence of the
upstream flow field. In Fig. 9(a), the triple point
region of the lifted flame has been enlarged to
examine the velocity field. The heat release rate
profiles are superimposed on the velocity vector
plots to locate the flame. A hypothetical vertical
line passing through the most upstream portion
of the flame is referred to as the center line.
Upstream of the triple point, the divergence of
the velocity field on both sides of the center line
is evident.

Two main effects influence the velocity asso-
ciated with the triple flame, namely, curvature
and heat release. Curvature of the partially
premixed front decreases the flame speed, while
the heat release increases this speed due to flow
dilatation. Figure 9(b) presents the streamwise
velocity profiles along four transverse locations
in the proximity of the center line. The heat
release causes the velocity component perpen-
dicular to the flame to increase so that the
streamlines bend inward toward the center line
as they cross the premixed reaction zones. This
creates a divergence in the velocity field up-
stream of the flame, causing the velocity to
reach a minimum value at the triple point. The
streamwise velocity at the triple point (identifi-
able through the heat release profile) is ≈ 0.45
m s^{-1}, whereas the velocity upstream of the
triple point equals 0.7 m s^{-1}. The velocity at the
location of the triple point is close to the
unstretched adiabatic laminar flame speed for a
stoichiometric methane–air flame (cf. [30]).
However, the overall propagating speed of the
triple flame equals the inflow velocity, i.e., 0.7 m
s^{-1}.

In this context, Dold [31] has proposed that
the triple flame propagation speed is bounded
by the maximum adiabatic laminar flame speed
of the system. Kioni et al. [13] have measured
the velocity of a lifted triple flame and found it
to be well above the adiabatic laminar flame
speed of the corresponding stoichiometric pre-
mixed fuel–air mixture. However, Ruetsch et al.
[4] have determined triple flame speeds that are
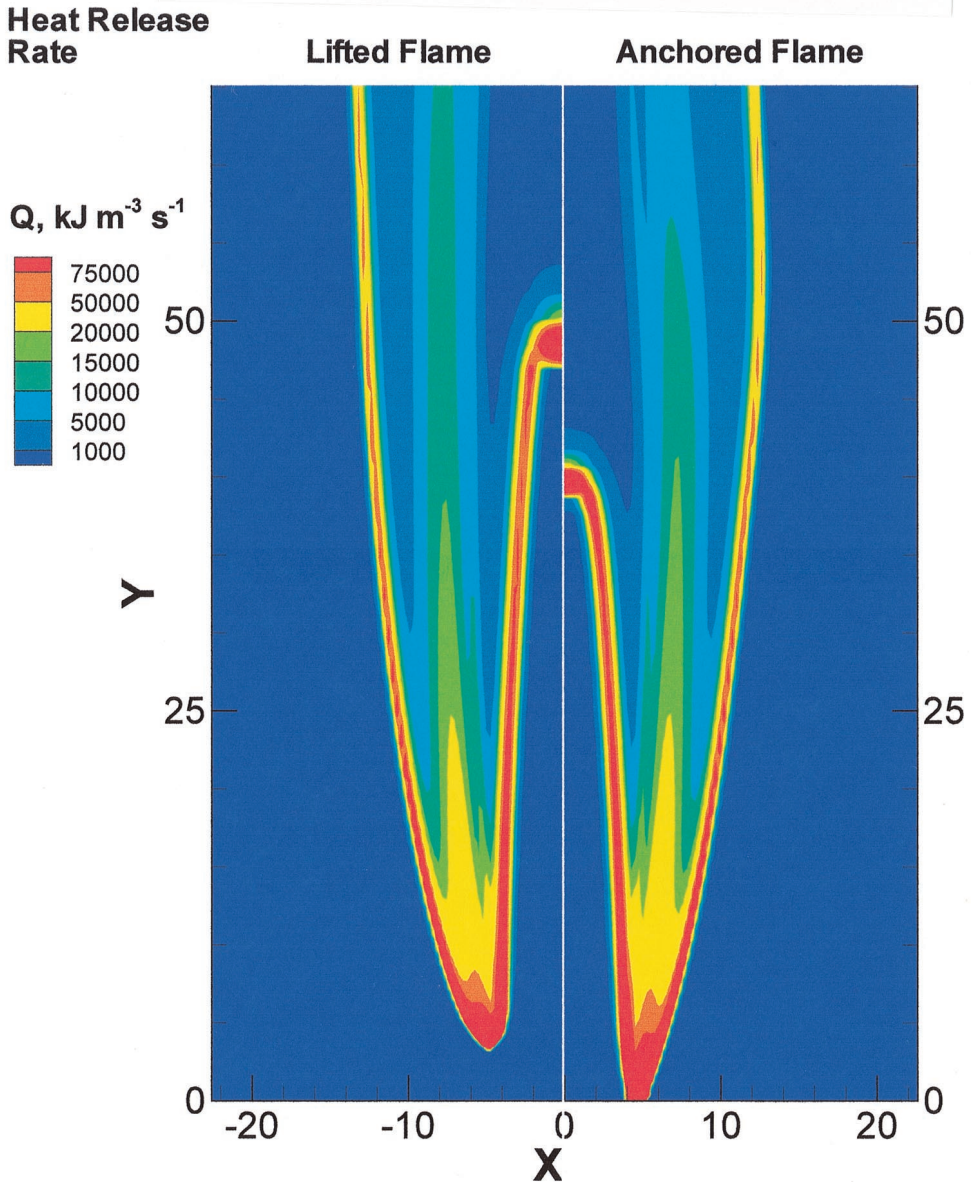higher than the corresponding planar premixed

Fig. 8. Comparison of the volumetric heat release rates (in units of kJ m^{-3} s^{-1}) of the lifted (left) and burner-stabilized (right) triple flames. The simulation conditions are $\phi_{in} = 1.8$, $\phi_{out} = 0.35$, $v_{in} = v_{out} = 0.7$ m s^{-1} for both cases. An infinitesimally thin splitter plate is considered for the lifted flame, while a 1.1 mm-thick wall is included during the simulation of the burner-stabilized flame.

flame speed. (This is in disagreement with Dold, but in agreement with the experimental results of Phillips [3].) They predicted that the minimum velocity, where the flame stabilizes, is close to the laminar flame speed S_L, but the overall flame speed of the triple flame, considered further upstream, is larger than S_L, both points being in agreement with our results.

Muniz and Mungal [32] experimentally investigated the velocity profile at the base of a lifted turbulent jet flame and also observed that the flame stabilizes itself in the region where the velocity is close to the premixed laminar flame speed. They found the instantaneous velocity at the stabilization point to vary between S_L–$3S_L$. Watson et al. [33] have also determined this
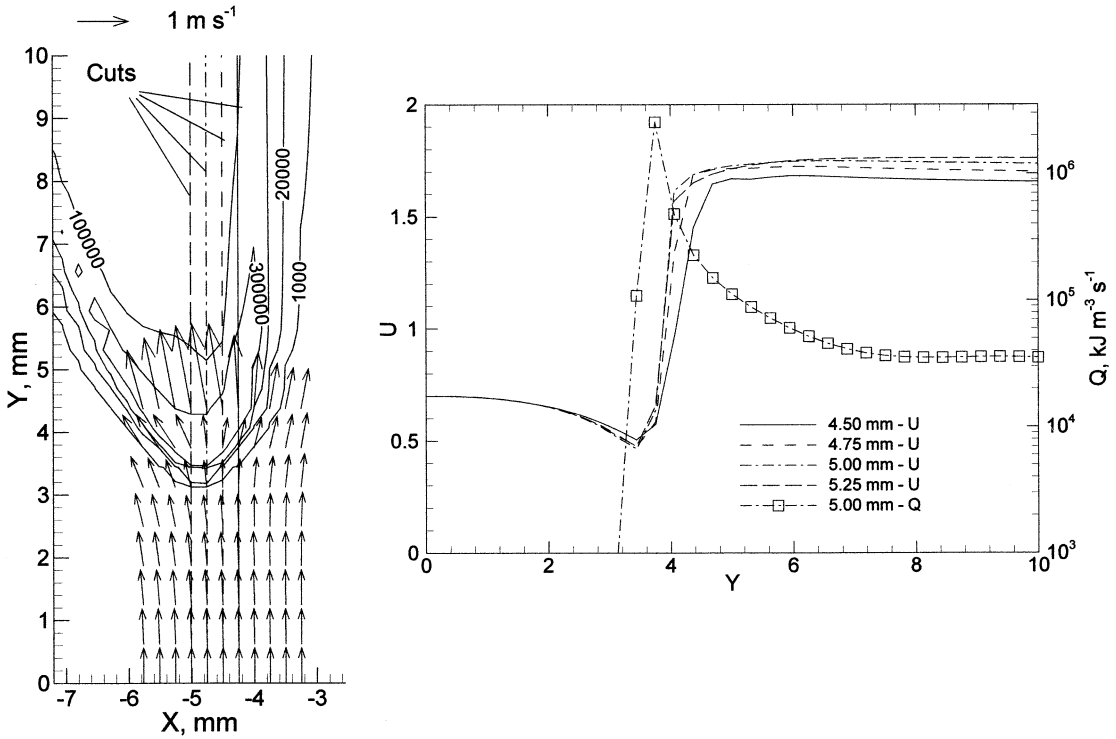
Fig. 9. (a) Velocity vectors superimposed on the heat release rate contours near the triple point for the simulated lifted flame: (b) Comparison of the streamwise velocity profiles at the four transverse displacements depicted in Fig. 8a. The heat release rate profile corresponding to the "centerline" streamwise profile at 5.0 mm is also shown.

velocity to be $\approx 3S_L$ (in a premixed region of a lifted flame), while Schefer and Goix [34] determined that the average velocity at the instantaneous flame base increased from $0.2S_L$–$1.2S_L$ with increasing Reynolds number. Our results are also consistent with these latter investigations. In future work we will address the behavior of this velocity as the equivalence ratio, the inlet velocity profile, and inlet mixture fraction are changed.

Similitude

We have shown that the flame structure of complex partially premixed flames in various configurations follows state relationships with respect to a modified conserved scalar $\xi = (Z - Z_l)/(Z_r - Z_l)$ [9, 24, 35] (although the approach assumes equal diffusivity of all species [36–38]). The value of ξ equals unity on the rich side, and is zero on the lean side. Here, Z denotes the local mixture fraction of an elemental species, and the subscripts r and l are

conditions relevant at the boundaries of the rich and lean regions, respectively.

State relationships are presented for the temperature, H-atom (radical), CO (intermediate), and CO_2 (product) mass fraction profiles in Fig. 10 along three sets of transverse locations with respect to ξ (defined in terms of the local nitrogen mass fraction) for both the burner stabilized and lifted flames. To avoid clutter, the heat release rate profile is superimposed on the figure at a single transverse location. The heat release rate profile clearly identifies the location of the three reaction zones, two of which are premixed, and the other nonpremixed.

The heat release distribution and the scalar profiles are virtually identical for both flames with respect to ξ, and attest to the overall similitude between the burner-stabilized and lifted flames. The profiles show that both flames exhibit a strikingly similar structure (in mixture fraction space). As in the burner-stabilized
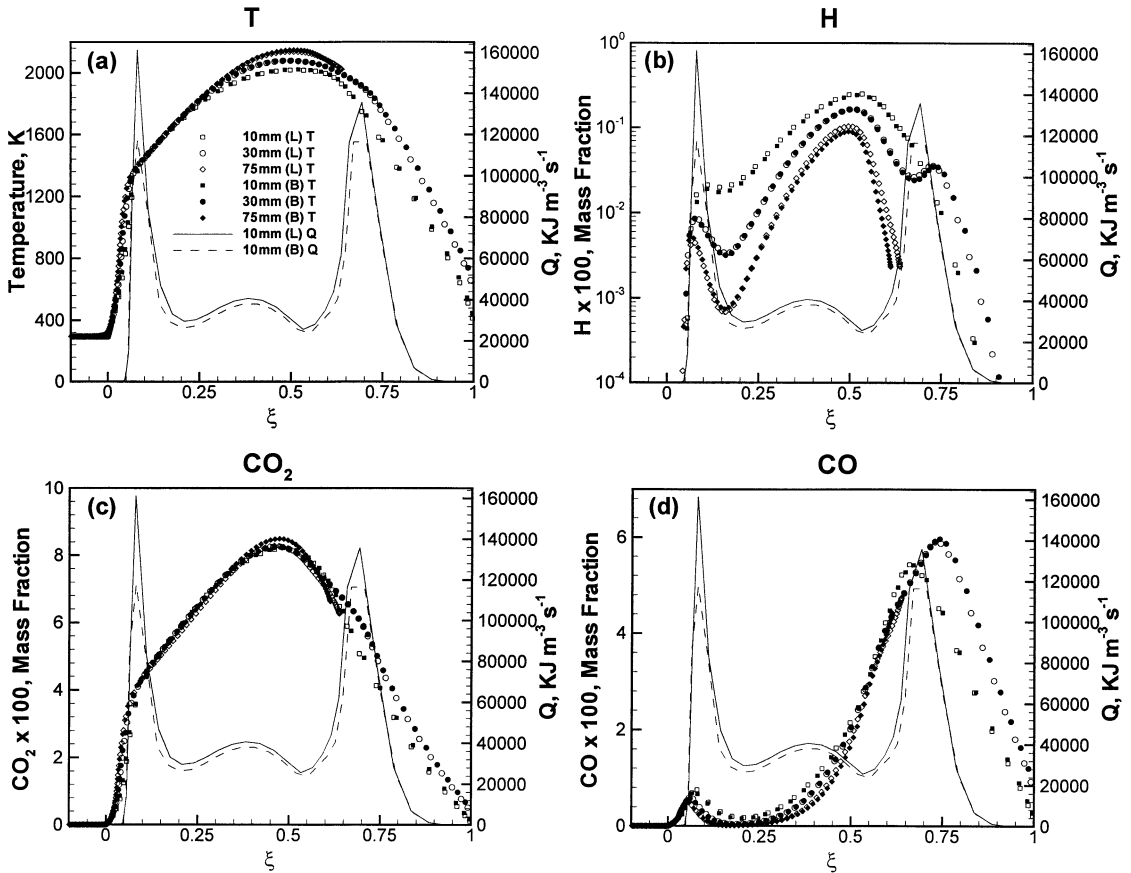
Fig. 10. Similitude between the burner-stabilized and lifted flames as illustrated though a comparison of the distribution of the heat release rates and various scalar profiles, such as those of temperature, H-atoms, CO, and CO_2.

flame, in the lifted flame also (1) radicals are produced in the vicinity of the three reaction zones, (2) CO and H_2 are produced in rich regions, and (3) they are consumed in nonpremixed-type regions where both species are, respectively, converted into CO_2 and H_2O.

The structure of the extremity of the nonpremixed reaction zone varies with the applied mixture fraction gradient. This gradient is negligibly modified by reducing the splitter wall thickness and, consequently, serves as a control in both the burner-stabilized and lifted flames. Therefore, while there is a small amount of heat transfer to the burner [1], the similarity between the burner-stabilized and lifted flames suggests that it has negligible influence. The thermal boundary condition at the burner inlet in the computational model is isothermal and not adiabatic, i.e., upstream diffusional heat transfer into the incoming gas is allowed to occur.

CONCLUSIONS

We have validated our simulations of burner-stabilized triple flames with detailed measurements. Thereafter, we have simulated lifted flames without significantly modifying the boundary conditions used for investigating the burner-stabilized flames.

1. In case of the burner-stabilized flame, the height of the inner reaction zone is well predicted, and the measured and predicted shapes and widths of the two outer (nonpremixed and lean premixed) reaction zones are in good agreement.

2. The measurements (using holographic inter-

feromety) and predictions of the temperature distribution are in excellent agreement. The region with the highest temperatures lies between the inner premixed and the central nonpremixed reaction zone. The high-temperature region appears to be slightly narrower in the laboratory flame due to burner edge effects.

3. There is good agreement between the scalar profiles that represent reactant (O_2, CH_4) consumption, intermediate (CO, H_2) formation followed by intermediate consumption and product (CO_2, H_2O) formation.

4. A lifted flame is obtained by creating a splitter wall of infinitesimal thickness, but with conditions otherwise unchanged from those corresponding to the burner-stabilized flame. Its flame height is larger, but the two flames otherwise exhibit remarkable similarity with respect to the shapes and separation distances regarding the three reaction zones, as well as the interactions between these three regions. The heat release distribution and the scalar profiles are virtually identical for both flames in mixture fraction space and attest to the similitude between the burner stabilized and lifted flames.

5. The heat release causes the velocity component perpendicular to the lifted flame to increase. Consequently, the streamlines begin to diverge upstream of the flame. This causes the velocity to reach a minimum value (≈ 45 cm s^{-1}) at the triple point, a value that is close to the unstretched adiabatic laminar flame speed for a stoichiometric methane–air flame. However, the overall propagation speed of the triple flame equals the inflow velocity in agreement with measurements made by other investigators.

REFERENCES

1. Azzoni, R., Ratti, S., Aggarwal, S. K., and Purl, I. K., *Combust. Flame* 119:23–40 (1999).
2. Azzoni, R., Ratti, S., Purl, I. K., and Aggarwal, S. K., *Phys. Fluids* 11:3449–3464 (1999).
3. Phillips, H., in *Tenth Symposium (International) on Combustion*, Cambridge, 1965, p. 1277.
4. Ruetsch, G. R., Vervisch, L., and Liñán, A., *Phys. Fluids* 7:1447 (1995).
5. Takahashi, F., Schmoll, W. J., and Katta, V. R., *Twenty-Seventh Symposium (International) on Combustion*, Pittsburgh, 1998, pp. 675–684.
6. Wichman, I., and Ramadan, B., *Phys. Fluids* 12:3145–3154 (1998).
7. Chung, S. H., and Lee, B. J., *Combust. Flame* 86:62 (1991).
8. Echekki, T., and Chen, J. H., *Combust. Flame* 114:231 (1998).
9. Aggarwal, S. K., and Puri, I. K., *AIAA J.* 36:1190 (1998).
10. Plessing, T., Terhoeven, P., Peters, N., and Mansour, M. S., *Combust. Flame* 115:335 (1998).
11. Buckmaster, J., and Matalon, M., *Twenty-Second Symposium (International) on Combustion*, Pittsburgh, 1988, p. 1527.
12. Domingo, P., and Vervisch, L., *Twenty-Sixth Symposium (International) on Combustion*, Pittsburgh, 1996, p. 233.
13. Kioni, P. N., Rogg, B., Bray, K. N. C., and Liñán, A., *Combust. Flame* 95:276 (1993).
14. Ratner, A., Driscoll, J. F., Donbar, J. M., Carter, C. D., Mullin, J. A., and Dahm, W. J. A., Paper presented at the 1999 Joint Meeting of the US Sections of The Combustion Institute, Washington, DC, March 15–17, 1999.
15. Shu, Z., Krass, B. J., Choi, C. W., Aggarwal, S. K., Katta, V. R., and Puri, I. K., *Twenty-Seventh Symposium (International) on Combustion*, Pittsburgh, 1998, pp. 625–632.
16. Vest, C. M., *Holographic Interferometry*, Wiley, New York, 1979.
17. Montgomery, G. P., and Reuss, D. L., *Appl. Optics* 21:1373 (1982).
18. Hertz, H. M., *Optics Commun.* 1:131 (1985).
19. Xiao, X., Choi, C. W., and Puri, I. K., Paper No. 137 presented at the 1999 Joint Meeting of the US Sections of The Combustion Institute, Washington, DC, March 15–17, 1999.
20. Xiao, X., Choi, C. W., Puri, I. K., *Combust. Flame* 120:318–332 (2000).
21. Huh, J. Y., Lee, K. Y., and Puri, I. K., *Combust. Flame* 96:381–392 (1994).
22. Ratti, S., MS Thesis, University of Illinois at Chicago, 1999.
23. Katta, V. R., Goss, L. P., and Roquemore, W. M., *Combust. Flame* 96:60 (1994).
24. Shu, Z., Aggarwal, S. K., Katta, V. R., and Puri, I. K., *Combust. Flame* 111:276 (1997).
25. Shu, Z., Choi, C. W., Aggarwal, S. K., Katta, V. R., and Puri, I. K., *Combust. Flame* 118:91–107 (1999).

26. Kee, R. J., Miller, J. A., and Warnatz, J., A Fortran Program Package for the Evaluation of Gas-phase Viscosities, Conductivities, and Diffusion Coefficients, Sandia National Laboratories Report SAND83-8209, 1983.

27. Peters, N., in *Reduced Kinetic Mechanisms for Applications in Combustion Systems*, Lecture Notes in Physics (N. Peters and B. Rogg, Eds.), Springer-Verlag, Berlin, Vol. m15, 1993, pp. 3–14.

28. McManus, K., Yip, B., and Candel, S., *Exp. Thermal Fluid Sci*. 10:486–502 (1995).

29. Najm, H., N., Paul, P. H., Mueller, C. J., and Wyckoff, P. S., *Combust. Flame* 113:312–332 (1998).

30. Egolfopoulos, F. N., Zhu, D. L., and Law, C. K., *Twenty-Third Symposium (International) on Combustion*, The Combustion Institute, Pittsburgh, pp. 471–478, 1990.

31. Dold, J. W., *Combust. Flame* 76:71 (1989).

32. Muniz, L., and Mungal, M. G., *Combust. Flame* 111:16 (1997).

33. Watson, K. A., Lyons, K. M., Donbar, J. M., and Carter, C. D., *Combust. Flame* 117:257–271 (1999).

34. R. W. Schefer, P. J. Goix, *Combust. Flame* 112:559 (1998).

35. Krass, B. J., Zellmer, B. W., Puri, I. K., and Singh, S., *ASME J. Energy Res. Technol*. 121:66–72 (1999).

36. Peters, N., *Twentieth Symposium (International) on Combustion*, The Combustion Institute, Pittsburgh, pp. 353–360, 1984.

37. Seshadri, K., Puri, I., and Peters, N., *Combust. Flame* 61:237–249 (1985).

38. Rogg, B., Behrendt, F., and Warnatz, J., *Twenty-First Symposium (International) on Combustion*, The Combustion Institute, Pittsburgh, PA, 1986, p. 1533.